Tellus
SERIES A
DYNAMIC
METEOROLOGY
AND OCEANOGRAPHY
PUBLISHED BY THE INTERNATIONAL METEOROLOGICAL INSTITUTE IN STOCKHOLM

Tellus (2011), 63A, 126–137

TELLUS

Using an ensemble of climate projections for simulating recent and near-future hydrological change to lake Vänern in Sweden

By JONAS OLSSON*, WEI YANG, L. PHIL GRAHAM, JÖRGEN ROSBERG and JOHAN ANDRÉASSON, *Swedish Meteorological and Hydrological Institute, 601 76 Norrköping, Sweden*

(Manuscript received 21 October 2009; in final form 6 July 2010)

ABSTRACT

Lake Vänern and River Göta älv in southern Sweden constitute a large and complex hydrological system that is highly vulnerable to climate change. In this study, an ensemble of 12 regional climate projections is used to simulate the inflow to Lake Vänern by the HBV hydrological model. By using distribution based scaling of the climate model output, all projections can accurately reproduce the annual cycle of mean monthly inflows for the period 1961–1990 as simulated using HBV with observed temperature and precipitation ('HBVobs'). Significant changes towards higher winter inflow and a reduced spring flood were found when comparing the period 1991–2008 to 1961–1990 in the HBVobs simulations and the ability of the regional projections to reproduce these changes varied. The main uncertainties in the projections for 1991–2008 were found to originate from the global climate model used, including its initialization, and in one case, the emissions scenario, whereas the regional climate model used and its resolution showed a smaller influence. The projections that most accurately reproduce the recent change suggest that the current trends in the winter and spring inflows will continue over the period 2009–2030.

1. Introduction

Climate change is expected to profoundly influence the hydrology of Sweden and northern Europe. The overall availability of water in Sweden is estimated to increase by 5–24% as a consequence of an increased total precipitation (Andréasson et al., 2004). Concerning river runoff, a changed annual pattern is expected towards higher flows in winter, a less pronounced snowmelt peak and lower summer flows. The changes will likely vary between different parts of Sweden, reflecting, for example, the influence of snow on the annual dynamics as well as geographical gradients of future changes in precipitation. These regional differences also govern the expected future changes in extreme high flows. In northern and central Sweden they are expected to decrease, as the highest flows there are generated by snowmelt. In southern Sweden, however, as the highest flows are generated by rainfall, they are likely to increase in line with the increased precipitation.

The main basis for performing hydrological climate change impacts assessment is to use output from global climate models (GCM). The results from GCM projections are influenced by a number of aspects, which contribute to uncertainty. One is the Intergovernmental Panel on Climate Change (IPCC) emissions scenario used (IPCC, 2007), which specifies expected future changes in greenhouse gas concentrations in the atmosphere based on various assumptions for future global development. Another is the GCM used, with its particular characteristics in terms of process descriptions and parameterizations, spatial and temporal resolution, etc. A third aspect is the initialization of the GCM, which may in particular influence the estimated near-future changes (i.e. some 20–30 years ahead). Over recent years, it has become common to apply a regional climate model (RCM) to dynamically downscale the GCM output to a higher spatial resolution in a limited region (e.g. Déqué et al., 2007; Jacob et al., 2007). In this case, the RCM properties will also influence results and add uncertainty.

One way to deal with different sources of uncertainty in impacts assessment is to use an ensemble of climate projections in the impacts modelling. This ensemble should, to the largest possible extent, cover all the aspects listed above, that is include different emissions scenarios, different GCMs, different GCM

*Corresponding author.
e-mail: jonas.olsson@smhi.se
DOI: 10.1111/j.1600-0870.2010.00476.x

initializations and different RCMs. In previous studies, such ensembles have not been readily available for assessment studies and generally only one or a few projections have been used for hydrological impacts, representing different emissions scenarios and/or models. However, Graham et al. (2007a,b) looked at hydrological impacts using a number of different RCM projections based on two GCM projections. They generally found that the different GCMs played a larger role than the different RCMs.

The main objective of this study is to explore how an ensemble of climate model projections can be used to increase confidence in near-future hydrological climate change impacts. We used an ensemble of 12 projections to drive the HBV hydrological model, set up and calibrated for Lake Vänern in south-western Sweden. The HBV model (Bergström, 1976) has been widely used for operational hydrological modelling in different regions and climates and is therefore suitably robust for climate change impact assessment (Section 3.1.1). The impact of different uncertainties involved are assessed, with respect to both reproducing inflow during the reference period 1961–1990 simulated using the HBV model with observed temperature and precipitation and, in particular, reproducing the change between this period and the period 1991–2008. Finally, based on these results, we interpret future projections for the period 2009–2030.

2. Catchment and data

2.1. Lake Vänern

Lake Vänern is the largest lake in Sweden and the third largest lake in Europe (Fig. 1). Via its main tributary, Klarälven, parts of Norway are included in its drainage basin, making it one of two major transboundary hydrological systems in Sweden (the other is Torneälven, bordering Finland in the north). Lake Vänern drains an area of some 47 000 km^2 into River Göta älv, the largest river in Sweden, which passes through Göteborg, the second largest city in Sweden, with a mean annual flow of 550 m^3 s^{-1}. Due to both its geographic location and influence on regional economics, Lake Vänern plays an important role in Swedish hydrology.

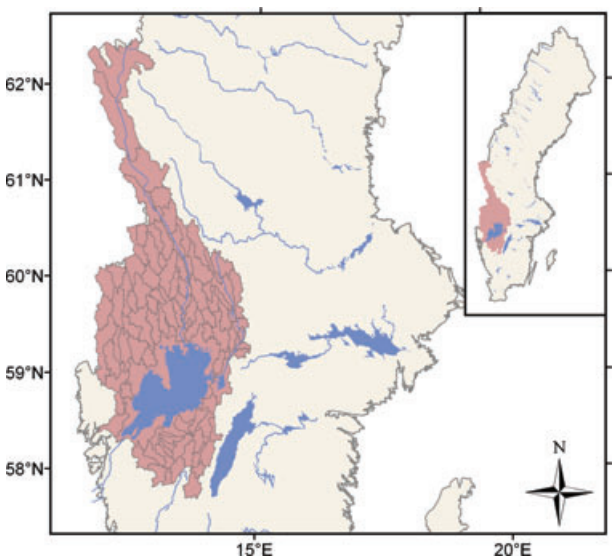

Fig. 1. The Lake Vänern catchment.

Lake Vänern and River Göta älv form a complex system with conflicting stakeholder interests and natural hazards, making it vulnerable to future climate changes (SOU, 2007). A dam with a controlled spillway is used to regulate the lake level, but in high-flow situations this regulation may not be sufficient for keeping the level below acceptable limits. There are several small cities along the lake that are today at risk for flooding with high lake levels. Furthermore, the shores of Lake Vänern and the downstream River Göta älv floodplain are under increasing pressure for expanded development of new residential areas. This would ultimately increase potential property and infrastructure damages and put a higher burden on emergency services during flooding events. Reducing lake levels by increasing discharge to the River Göta älv is problematic as this could trigger landslides and cause increased flooding in the vicinity of the river mouth. Conversely, sustained lower water levels in Lake Vänern could have negative consequences such as disturbed ecosystems, navigation difficulties and decreased hydropower potential (see further Bergström et al., 2007).

This study focuses on the inflow to Lake Vänern since 1961 and in particular changes occurring during this period. To characterize these changes, the available period was divided into two subperiods: 1961–1990 and 1991–2008. The former was chosen as it is an established reference period in Sweden and thus facilitates interpretation of the results from this study with respect to earlier work. It may be remarked that a division into equally sized subperiods would have been slightly superior with respect to identifying statistically significant changes, but we prefer keeping the established reference period.

As compared with the reference period, the mean annual temperature during 1991–2008 has increased by 1.0°C (Table 1). The temperature has increased in all seasons but most clearly in winter (2.1°C); in other seasons the increase is lower than the mean annual increase. Precipitation has increased in all seasons except autumn in which it has decreased slightly (Table 1). The mean annual increase is 58 mm, corresponding to 7.5%.

As daily inflow to Lake Vänern is difficult to estimate accurately from observations, it has been simulated using a well-calibrated set-up of the HBV model (Section 3.1) with observed precipitation and temperature. This simulation is hereafter referred to as 'HBV-observed' ('HBVobs'), to distinguish it from the HBV simulations based on RCM projections.

In the reference period 1961–1990, a pronounced snowmelt-generated spring flood peak in early May is evident, followed by a decrease during late spring and early summer to an annual minimum in July to August (Fig. 2). In autumn, the inflow increases to reach a rather stable level during the winter, until the snowmelt

Table 1. Mean observed temperature and precipitation for the periods 1961–1990 (P1) and 1991–2008 (P2), and the difference (Δ)

	Winter			Spring			Summer			Autumn			Annual		
	P1	P2	Δ	P1	P2	Δ	P1	P2	Δ	P1	P2	Δ	P1	P2	Δ
T (°C)	−4.8	−2.7	2.1	3.8	4.7	0.9	14.4	15.0	0.6	5.3	5.7	0.4	4.7	5.7	1.0
P (mm)	157	184	27	144	158	14	230	261	31	245	231	−13	775	855	58

Note: Winter is defined as December–February, spring as March–May, summer as June–August and autumn as September–November.

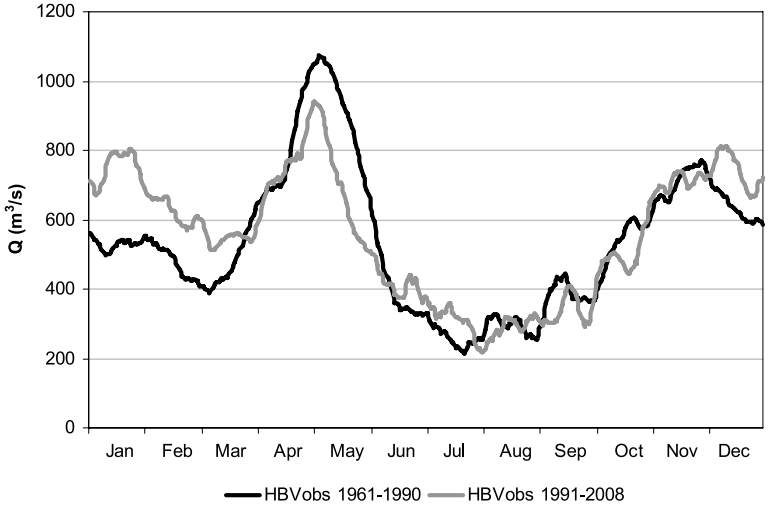

Fig. 2. HBV-simulated daily inflow to Lake Vänern using observed temperature and precipitation (HBVobs) for the periods 1961–1990 and 1991–2008.

begins again in late March. Simulated inflow during the recent period 1991–2008 differs from this pattern during winter and spring (Fig. 2). In winter, January in particular, the inflow is higher, whereas the spring flood shows shorter duration and a lower peak. The changes are qualitatively in line with the observed warming (Table 1), resulting in more precipitation falling as rain rather than snow during the winter and consequently a thinner snow pack at the start of the snowmelt period.

2.2. *Climate projections*

An ensemble of 12 climate model projections was used in this work. All were downscaled from GCMs using RCMs. As shown in Table 2, projections from four different RCMs were used, driven by three different GCMs. Most of the RCMs used a common limited domain over Europe that includes all of the Nordic Region (van der Linden and Mitchell, 2009). Only scenarios E3R25A1Ba and E3R25A2 used a somewhat different domain that extends further westward (covering more of the Atlantic Ocean). More details on the models and projections used can be found in Kjellström et al. (2010).

Half of the RCM simulations were conducted at a horizontal resolution of 25 km and half at 50 km. A mini-ensemble is also included whereby three different initializations of global projections were made by the same GCM. Most of the climate projections are based on the A1B emissions scenario from IPCC (IPCC, 2007), but the A2 and B1 emissions scenarios are also represented. Scenario A2 leads to a relatively high increase of the global surface mean temperature by the end of the century, B2 a relatively low increase, and A1B represents an intermediate situation (IPCC, 2007). In the abbreviations used in the following, the first two characters denote the GCM (and initialization member, when applicable), the following three the RCM (and resolution, when applicable) and the final characters denote the emissions scenario (Table 2).

3. Methods

3.1. *Inflow simulations*

3.1.1. Hydrological model. The HBV model (Bergström, 1976, 1992; Lindström et al., 1997) is a rainfall-runoff model that includes conceptual numerical descriptions of hydrological processes at the catchment scale. HBV has been applied in more than 40 countries all over the world, including countries with quite different climatic conditions such as, for example, Sweden, Zimbabwe, India and Colombia. HBV has been applied for scales ranging from lysimeter plots (Lindström and Rodhe,

Table 2. List of climate projections used

GCM	Initialization member	RCM	Resolution (km)	IPCC	Abbreviation
ECHAM5	3	RCA3	25	A1B	[a]E3R25A1Ba
ECHAM5	3	RCA3	25	A2	E3R25A2
ARPEGE	–	ALADIN	25	A1B	ARALAA1B
ECHAM5	3	RACMO	25	A1B	E3RACA1B
ECHAM5	3	REMO	25	A1B	E3REMA1B
CCSM3	–	RCA3	50	A1B	CCR50A1B
ARPEGE	–	RCA3	50	A1B	ARR50A1B
ECHAM5	1	RCA3	50	A1B	E1R50A1B
ECHAM5	1	RCA3	50	B1	E1R50B1
ECHAM5	2	RCA3	50	A1B	E2R50A1B
ECHAM5	3	RCA3	50	A1B	E3R50A1B
ECHAM5	3	RCA3	25	A1B	*E3R25A1Bb

Note: See also Kjellström et al. (2010) and van der Linden and Mitchell (2009).
[a]These two projections are identical with respect to the properties in the table, but differ with respect to model domain and setup.
Model origins:
ECHAM5—Max-Planck-Institute for Meteorology, Hamburg, Germany
ARPEGE—Meteo-France, Toulouse, France
CCSM3—NCAR Community Climate System Model, Boulder, Colorado, USA
RCA3—Rossby Centre, Swedish Meteorological and Hydrological Institute (SMHI), Norrköping, Sweden
ALADIN—Meteo-France and the weather services of Bulgaria, Czech Republic, Hungary and Romania.
RACMO—Royal Netherlands Meteorological Institute (KNMI), De Bilt, The Netherlands
REMO—Max-Planck-Institute for Meteorology, Hamburg, Germany

1992) to the entire Baltic Sea drainage basin (Graham, 1999). The model is used for flood forecasting in the Nordic countries. It has also been extensively used for other purposes, such as spillway design flood simulation (Bergström et al., 1992), water quality modelling (Arheimer and Brandt, 1998) and impact studies for climate change assessments (e.g. Bergström et al., 2001; Andréasson et al., 2004; Arheimer et al., 2005).

The general water balance in the HBV model can be described as

$$P - E - Q = \frac{\mathrm{d}}{\mathrm{dt}} \left[SP + SM + UZ + LZ + \text{lakes} \right], \qquad (1)$$

where P is precipitation, E is evapotranspiration, Q is runoff, SP is snow pack, SM is soil moisture, UZ is the content of the upper groundwater zone, LZ is the content of the lower groundwater zone and 'lakes' is the lake volume. Input data are observations of precipitation, air temperature and estimates of potential evapotranspiration. The time step is typically 1 day, as used here. Air temperature data are used for calculations of snow accumulation and melt. It can also be used to calculate potential evapotranspiration, or to adjust the long-term mean monthly potential evapotranspiration into daily time series when the temperatures deviate from normal values.

The model consists of subroutines for meteorological interpolation, snow accumulation and melt, evapotranspiration estimation, soil moisture accounting, runoff generation and finally, a simple routing procedure between subbasins and in lakes. For subbasins of considerable elevation range, a subdivision into elevation zones is typically made, which is used for the snow and soil moisture routines. This allows for lapse rate calculations to be made for temperature dependent processes, such as the snow routine. Each elevation zone can further be divided into different vegetation zones (e.g. forested and non-forested areas). Applying the model necessitates calibration of a number of free parameters (around 10 in the present application).

The HBV model setup used in this study is the current operational forecast model that SMHI setup for use by the hydropower company, Vattenfall AB, to optimize the regulation of Lake Vänern. In the setup, the catchment of Lake Vänern is divided into 96 subbasins, which have been regionally calibrated using runoff observations from 17 stations. Input data are areal precipitation and temperature calculated using optimal interpolation (Johansson, 2000; Johansson and Chen, 2003). Daily potential evapotranspiration is calculated using a simple temperature-index method based on Thornthwaite's approach (Lindström et al., 1994, 1997). An example of performance in

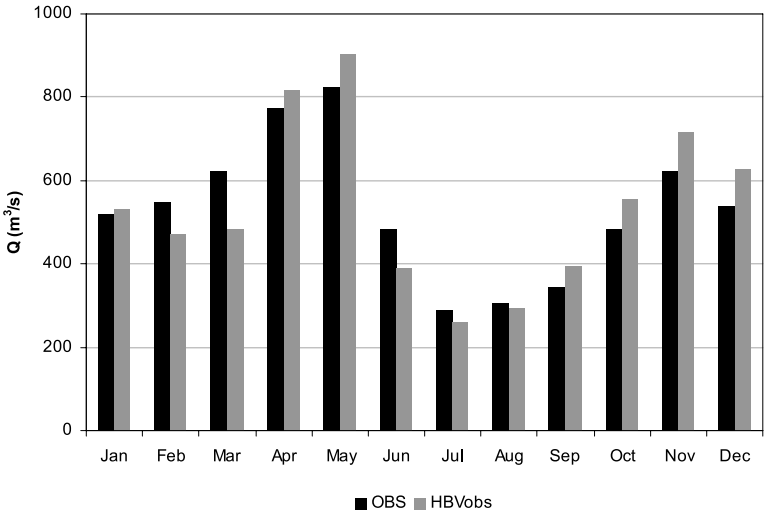

Fig. 3. Mean monthly discharge at Vargön for the reference period 1961–1990: observed (OBS) and HBV simulated with observed temperature and precipitation (HBVobs).

the reference period is shown in Fig. 3, for the outlet of Lake Vänern at Vargöns powerplant. The annual volume error is 1.2% and the mean absolute monthly volume error is 12.3%.

3.1.2. Climate model adjustments. Because of systematic climate model errors, some form of adjustment is generally required in the raw climate model output before use in hydrological simulations. This is necessary to obtain realistic, credible hydrological results. The distribution based scaling (DBS) approach developed by Yang et al. (2010) was used in this study to improve outputs from the climate change projections. It has been applied to all RCM projections available to date from the ENSEMBLES Project (Ensemble-based Predictions of Climate Changes and their Impacts, see Section 6) for different hydrological response studies.

In the DBS approach, two primary hydrological variables, precipitation (P) and temperature (T), from climate model projections are adjusted before being used for HBV simulations. Observed daily P and T time series for the reference period 1961–1990 are used as a base to derive the respective scaling factors for the RCM P and T outputs from the corresponding time period of the climate projection. The function of the scaling factors is to adjust RCM outputs to make them statistically comparable to observations, in terms of mean and standard deviation. They are then applied to the rest of climate projection as it extends into the future. This correction assumes that the biases are systematic and constant for the entire climate projection.

For precipitation, two separate gamma distributions are implemented. One gamma distribution is for low-intensity precipitation events, and the other for extreme precipitation. The lower gamma distribution represents precipitation up to the 95th percentile of total precipitation events; the upper distribution represents events above the 95th percentile. The gamma distribution is a two-parameter distribution with the shape parameter, α, and the scale parameter, β. The product of $\alpha\beta$ describes the mean value of the studied data set, and $\alpha\beta^2$ shows the variance. Both mean and variance are calculated for RCM raw output and observations, respectively. The deficit in mean and ratio in variance can therefore be used as indices of the resulting improvement from applying the DBS approach.

Compared to precipitation, adjusting daily temperature is less complex. It is described by a Gaussian distribution with mean, μ, and standard deviation, σ. The distribution parameters are smoothed over the reference period using a 15-day moving window. Separate distribution parameters are calculated for precipitation days and non-precipitation days to take into account the dependence between P and T. As with precipitation, the resultant scaling factors are subsequently applied to the climate projections.

3.2. Evaluation

To characterize the level of adjustment required for precipitation using the DBS approach, we define a variable SS representing 'scaling strength' of the mean adjustment according to

$$SS = \frac{1}{N}\sum_{i=1}^{N} abs\left[\left(\alpha^i_{RCM}\beta^i_{RCM}\right) - \left(\alpha^i_{OBS}\beta^i_{OBS}\right)\right], \quad (2)$$

where α and β are parameters of the gamma distribution (Section 3.1), *RCM* and *OBS* denote simulated and observed precipitation in the reference period 1961–1990 and i denotes the ith model grid box covering the Lake Vänern catchment ($1 \leq i \leq N$). The value of *SS* increases with increasing difference between simulated and observed precipitation in the reference period. Therefore, the lower the value of *SS*, the lower the degree of adjustment needed. The analysis was performed separately for values below ($SS_{<95}$) and above ($SS_{>95}$) the 95th percentile.

The accuracy of the DBS-adjusted precipitation was evaluated using the root mean square error of integer percentiles in the

frequency distribution, that is

$$RMSE_P = \sqrt{\frac{1}{101}\sum_{p=0}^{100}\left(P^p_{RCM} - P^p_{OBS}\right)^2}, \quad (3)$$

where P^p denotes the pth percentile in the precipitation frequency distribution.

To evaluate the performance of the inflow simulations, we use the root mean square error of monthly mean discharge according to

$$RMSE_Q = \sqrt{\frac{1}{12}\sum_{m=1}^{12}\left(Q^m_{RCM} - Q^m_{HBVobs}\right)^2}, \quad (4)$$

where Q^m denotes either (1) the mean inflow in month m or, in comparison between periods 1961–1990 and 1991–2008, (2) the difference in mean monthly inflow. The value of $RMSE_Q$ is used to give the projections a rank R with respect to the accuracy of the simulated difference in inflow between the two periods.

As the evaluation includes the change in inflow between two periods, one key issue is whether this change is statistically significant or not. To make this assessment, t-testing was used to evaluate the hypothesis that the mean monthly inflow in the latter period (1991–2008) is significantly different from that in the former (1961–1990).

The t-test assumes that the sample has a normal distribution, and this issue was investigated using the Lilliefors test (Lilliefors, 1967). In the reference period, for eight out of 12 months the hypothesis of a normal distribution could not be rejected at the standard significance level 0.05. For three of the remaining months (January, June, August), the hypothesis was rejected at level 0.05 but not rejected at some lower level of significance (0.01–0.04). Only for September was the hypothesis of a normal distribution entirely rejected. Considering the small sample used we assume that the rejection is largely influenced by sampling variability and that the overall results of the Lilliefors testing indicate that the HBVobs simulations are well characterized by a normal distribution and that the t-test thus can be meaningfully applied in our case.

To evaluate the performance of the projections in terms of significant monthly changes, we use two measures commonly used in the verification of categorical forecasts: hit rate (HR) and false alarm rate (FAR; e.g. Wilks, 1995). In this case, a 'hit' refers to the case where a projection correctly reproduces a significant monthly change found in the HBVobs simulations. Similarly, a 'false alarm' implies that a projection erroneously indicates a significant change for a month in which observations do not indicate any.

To quantify the amount of variability in the results associated with a certain uncertainty sources, we use the average standard deviation of the monthly discharge projections according to

$$SD = \frac{1}{12}\sum_{m=1}^{12}\left[\sqrt{\frac{1}{CP-1}\sum_{i=1}^{CP}\left(Q^{mi}_{RCM} - \frac{1}{CP}\sum_{i=1}^{CP}Q^{mi}_{RCM}\right)^2}\right] \quad (5)$$

where i denotes the ith out of a total CP climate projections used in the assessment of this source. The value of SD increases with increasing difference between the projections, indicating the impact of the uncertainty source considered.

4. Results and discussion

Table 3 contains the overall results of the study in terms of numerical performance measures. Concerning the scaling strength of low/medium-intensity rainfall, $SS_{<95}$, almost all projections are contained within a limited range of 0.8–1.0. Only projection E3R25A1Ba stands out with a lower value, indicating better agreement with observed precipitation than the other

Table 3. Total results in terms of *SS*, *RMSE*, *R*, *HR* and *FAR*

Scenario	$SS_{<95}$	$SS_{>95}$	$RMSE_P$	$RMSE_{Q\mathrm{ref}}$	$RMSE_{Q\Delta}$	$R_{Q\Delta}$	*HR*	*FAR*
E3R25A1Ba	0.67	1.71	0.249	41.2	98.4	5	1/3	2/9
E3R25A2	0.90	1.62	0.166	33.0	146.4	11	1/3	0/9
ARALAA1B	0.79	2.23	0.209	76.3	92.8	2	0/3	3/9
E3RACA1B	0.81	2.17	0.165	41.9	124.4	8	1/3	2/9
E3REMA1B	0.85	1.73	0.173	40.1	105.4	6	2/3	4/9
CCR50A1B	1.09	3.55	0.138	50.9	95.5	4	2/3	3/9
ARR50A1B	0.83	2.58	0.220	50.3	94.9	3	1/3	3/9
E1R50A1B	0.96	2.18	0.237	51.1	136.7	10	0/3	0/9
E1R50B1	0.96	2.22	0.229	51.2	153.3	12	0/3	1/9
E2R50A1B	0.89	2.07	0.193	42.7	87.0	1	1/3	0/9
E3R50A1B	0.87	2.09	0.153	48.7	135.5	9	2/3	4/9
E3R25A1Bb	0.88	1.71	0.189	45.9	106.0	7	2/3	3/9

Note: Subscript 'ref' denotes performance in the reference period 1961–1990; 'Δ' denotes the difference for 1991–2008 compared to 1961–1990. The denominator in *HR* (*FAR*) represents the maximum number of 'hits' ('false alarms').

projections. The value of $SS_{>95}$ exhibits a wider spread with more than a factor of two differing between the minimum and the maximum. Overall the projections are rather similar in terms of *SS*, and there is a weak correlation between the two *SS* values, that is projections tend to be 'good' (or 'bad') with respect to both low/medium and extreme intensities. It can be noted that projection CCR50A1B requires the strongest DBS adjustment for all precipitation intensities.

The accuracy of the DBS-adjusted precipitation as characterized by $RMSE_P$ varies between 0.138 and 0.249 (Table 3). In fact, the largest error was obtained for projection E3R25A1Ba, which was one of the projections requiring least adjustment as estimated using *SS*. Overall there is a weak tendency of inverse proportionality between *SS* and $RMSE_P$, that is the more adjustment required the higher is the accuracy of the adjusted precipitation. Further research is needed to investigate whether this is a pure coincidence or a generic feature of the DBS approach and, in case of the latter, to identify the reason.

After the application of DBS, the intra-annual discharge cycle is well represented in all projections (Fig. 4) with $RMSE_Q$ being generally in the range 40–50 $m^3\ s^{-1}$. The best performance overall was found for projection E3R25A2, which is also the projection that best captures the spring flood peak in May. Projection ARALAA1B has a markedly higher $RMSE_Q$, and as seen in Fig. 4 it overestimates discharge in mid-winter (January–February) and then underestimates the spring flood peak as well as the discharge in late summer and throughout autumn. This feature, as well as the overall spread between the projections in Fig. 4, represents the limitations of the DBS method with respect to reproducing the observed climate. There is no clear relationship between $RMSE_P$ and $RMSE_Q$, that is the accuracy of the DBS-adjusted precipitation does not appear to substantially influence the accuracy of the inflow simulations.

The performance between the different projections varies widely with respect to simulating the changes in monthly mean discharge from 1991 to 2008 compared to 1961 to 1990 (Fig. 5). In general, the projections qualitatively reproduce the changes found in HBVobs during the beginning of the year with an increase in the discharge during winter and early spring (December–March) and a decrease during the main spring flood period (April–May). This indicates a good reproduction of changes in both the evolution of the snow pack during winter and the timing of the snowmelt in spring. All projections however underestimate the increase in Jan-Feb and most overestimate it in Mar. During the rest of the year (June–November) most scenarios are somewhat out-of-phase with the changes in HBVobs. In summer (June–August) HBVobs shows a weak increase but most projections indicate a decrease; in autumn (September–November) the situation is the opposite, that is HBVobs shows a decrease but projections generally increase. As discharge in summer and autumn are mainly controlled by rainfall, these discrepancies indicate that the projections underestimate rainfall in summer and overestimate it in autumn for the period 1991–2008. In summer the underestimated discharge may also be related to overestimated temperature and consequently higher evapotranspiration.

The different accuracies reached by the different projections are manifested also in the $RMSE_Q$, which varies between 87.0 and 153.3 $m^3\ s^{-1}$ ($RMSE_{Q\Delta}$, Table 3). The best performance is found for projection E2R50A1B. This projection underestimates the increase during January to March but for the rest of the year reproduces well the overall pattern in HBVobs with a reduced

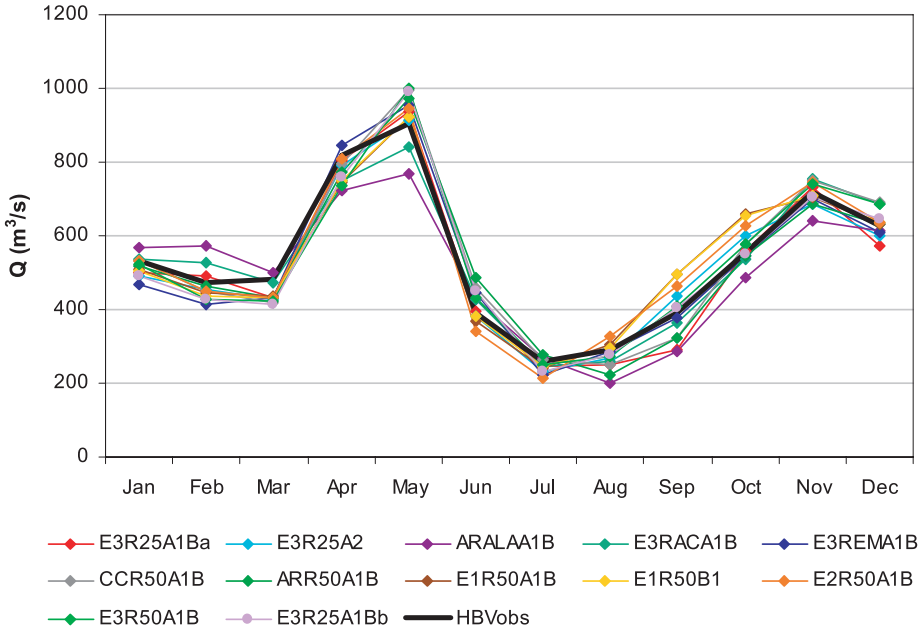

Fig. 4. HBV-observed (HBVobs) and simulated mean monthly inflow to Lake Vänern for 1961–1990.

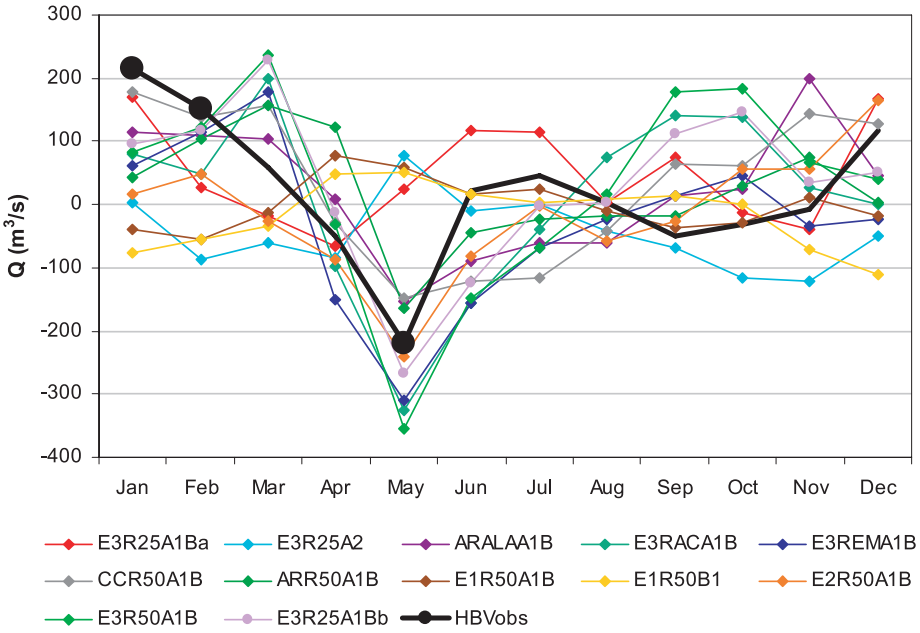

Fig. 5. HBV-observed (HBVobs) and simulated difference in mean monthly inflow to Lake Vänern for 1991–2008 compared to 1961–1990. For HBVobs, a circle indicates statistically significant change.

spring flood and rather stable conditions in summer and autumn. The least accurate projection in terms of $RMSE_Q$, E1R50B1, is characterized by a decrease in winter discharge and an increase of the spring flood, that is completely opposite to the pattern in HBVobs (the stable conditions in summer and autumn are, however, well reproduced).

Considering the categorical evaluation measures *HR* and *FAR*, three monthly changes in HBVobs were found to be statistically significant: the increase in January–February and the decrease in May. *HR* can thus be used to show how many of these three that a certain projection reproduces. No projection reproduces all three, but four projections reproduce two of them (Table 3). These projections also have, however, a high *FAR* of 3/9 or 4/9, that is they tend to generate significant changes also in months when in reality there was not any. This is known as high 'sharpness' in forecast verification, that is the projected values deviate sharply from the climatology (e.g. Wilks, 1995). Several projections also demonstrate a low sharpness, in particular E1R50A1B for which both *HR* and *FAR* are 0, that is it did not indicate any significant monthly change at all from the situation in 1961–1990.

4.1. Assessment of uncertainty sources

In the following we focus the evaluation separately on the different sources of uncertainty covered in the projection ensemble: GCM, GCM initialization, RCM, IPCC emissions scenario and RCM spatial resolution. In each figure (Figs 6–8), the projections included are identical except for one source of uncertainty that varies. Note that in the figures solid bars indicate statistically significant monthly changes and striped bars changes that are not significant.

Figure 6 shows the results from three projections differing in only the GCM used: CCSM3 (CCR50A1B), ARPEGE (AAR50A1B) and ECHAM5 (E3R50A1B). Overall, all projections describe reasonably well the changes in HBVobs in winter and spring, both in a qualitative (i.e. with respect to the sign of the change) and a quantitive (i.e. with respect to the magnitude of the change) sense. In summer and autumn, however, the projected changes generally have both the wrong sign and the wrong magnitude. The projections generated by CCSM3 and ECHAM5 have a markedly higher sharpness than the one generated by ARPEGE.

Figure 7 shows the results from three projections differing in only the GCM initialization using ECHAM5: member 1 (E1R50A1B), member 2 (E2R50A1B) and member 3 (E3R50A1B). In this case the differences between the projections are larger, both qualitatively and quantitatively. There are striking differences in performance between winter–spring and summer–autumn. Member 1 reproduces very well the changes in HBVobs (small) in summer and autumn, but fails to capture the changes (large) in winter and spring; for member 3, the situation is entirely opposite. Also the sharpness varies widely, being very low for member 1 and very high for member 3.

Figure 8 shows the results from three projections differing in only the RCM used: RACMO (E3RACA1B), REMO (E3REMA1B) and RCA3 (E3R25A1Bb). Overall the projections agree qualitatively and often also quantitatively; there are no clear differences in terms of sharpness. The difference in performance between winter–spring and summer–autumn

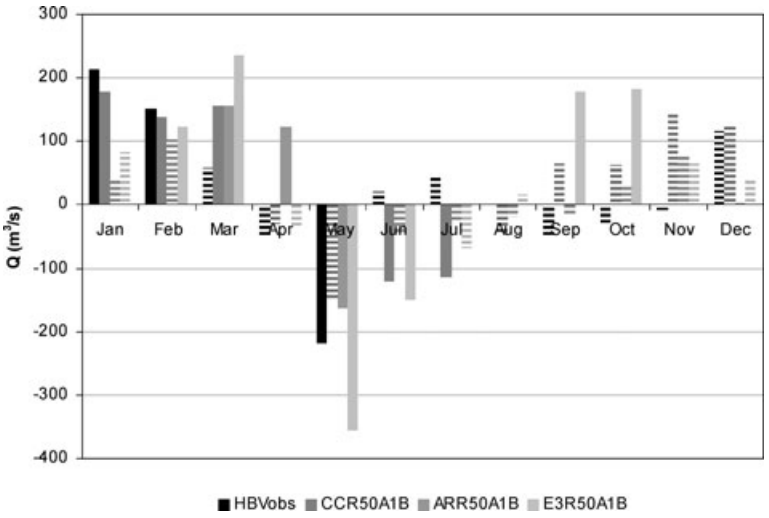

Fig. 6. Influence of GCM: difference in mean monthly inflow for 1991–2008 compared to 1961–1990, HBV-observed (HBVobs) and simulated using projections CCR50A1B, ARR50A1B and E3R50A1B. Solid bar indicate a statistically significant change.

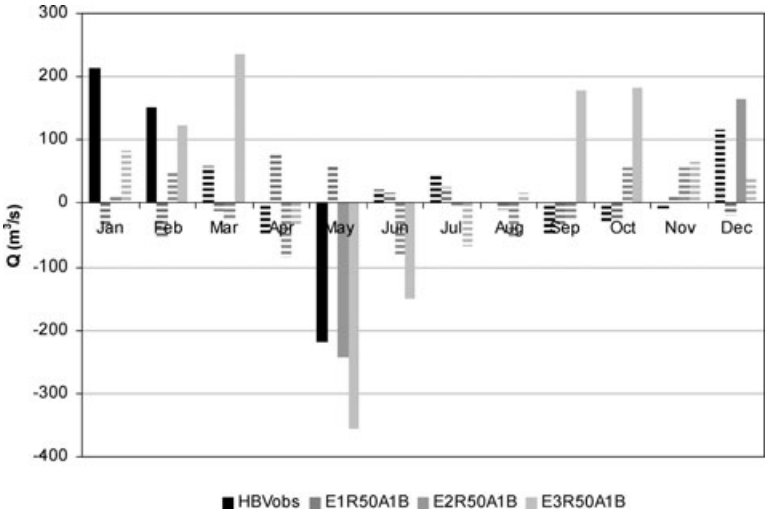

Fig. 7. Influence of GCM initialization: difference in mean monthly inflow for 1991–2008 compared to 1961–1990, HBV-observed (HBVobs) and simulated using projections E1R50A1B, E2R50A1B and E3R50A1B. Solid bar indicate a statistically significant change.

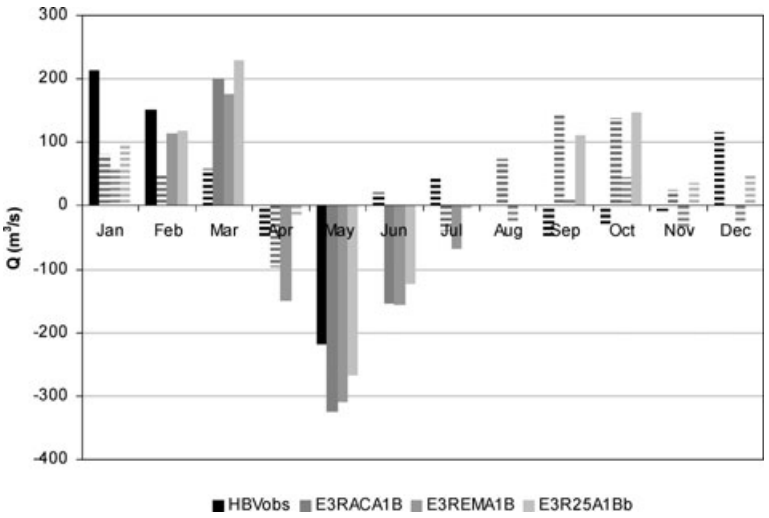

Fig. 8. Influence of RCM: difference in mean monthly inflow for 1991–2008 compared to 1961–1990, HBV-observed (HBVobs) and simulated using projections E3RACA1B, E3REMA1B and E3R25A1Bb. Solid bar indicate a statistically significant change.

Table 4. The impact of different uncertainty sources as estimated by *SD* (the numbers in parentheses denote the number of realizations available for this source)

	GCM	GCM initialization	RCM	RCM resolution	IPCC
SD	62.7 (3)	92.7 (3)	40.3 (3)	22.4 (2)	72.7/22.9 (2/2)

previously found for the third ECHAM5 member with emissions scenario A1B (projection E3R50A1B in Figs 6 and 7) is generally present also in these projections, which indicates that the RCM can generally not improve results in this respect. The only exception occurs in autumn, when REMO performs somewhat better than the other RCMs.

Two sets of projections differing in only the IPCC emissions scenario used—(1) A1B (E3R25A1Ba) and A2 (E3R25A2) and (2) A1B (E1R50A1B) and B1 (E1R50B1)—exhibit quite different results (not shown). In the former case, the monthly projections differ substantially and the IPCC emissions scenario appears to have a strong influence, but in the latter case the projections are overall in close agreement. This suggests that the difference between IPCC scenarios B1 and A1B, in terms of hydrological impacts in Lake Vänern, is smaller than the difference between scenarios A2 and A1B.

The final uncertainty source considered is horizontal RCM spatial resolution, through projections E3R50A1B (50 km) and E3R25A1Bb (25 km). The differences between the monthly projections (not shown) are small and it can be concluded that resolution has a minor impact in this case. There is, however, a weak tendency of higher sharpness in the 50 km projection.

The values of *SD* indicate that the influence of GCM initialization is the largest source of uncertainty, followed by GCM model used, RCM model used and finally RCM spatial resolution, which has the smallest influence (Table 4). Concerning the impact of the IPCC emissions scenario, the results are contradictory; in one case the influence was larger than the GCM used (A2 versus A1B), but in the other similar to the impact of spatial resolution (B1 versus A1B).

4.2. *Future projections*

Overall the projections of the difference in monthly mean inflow from 1991–2008 to 2009–2030 indicate a further increase of the discharge in winter and a decrease in summer and autumn (Fig. 9). In spring, there is a large variation with some projections, indicating a further decrease of the spring flood but also some indicating an increase, that is opposite to the recent trend.

Focusing on the three assumed most reliable projections, they consistently indicate that the current trend towards higher winter discharge and lower spring flood will continue over the coming 20 years at a similar pace (Fig. 9). These three projections further suggest that the stable conditions in summer and autumn will continue, in some contrast with the decreased discharge indicated by the total ensemble.

5. Summary and conclusions

The main findings of this study can be summarized as follows:

(1) In the period 1961–1990, the annual cycle of inflow to Lake Vänern is characterized by a snowmelt-generated peak in spring and a rainfall-generated secondary peak in late autumn. This cycle can be accurately reproduced by using the HBV model with inputs of daily precipitation and temperature from RCMs adjusted using distribution based scaling.

(2) Compared with the period 1961–1990, the period 1991–2008 is in particular characterized by a significantly increased inflow in mid-winter (January–February) and a decreased spring flood peak (May). No significant changes were found in summer and autumn.

(3) The accuracy with which RCM projections reproduce these changes vary. Most projections qualitatively reproduce the changes in winter and spring, but many indicate changes also in summer and autumn.

(4) The GCM used and its initializations are the largest sources of uncertainty, whereas the RCM used and its resolutions have a smaller influence. The influence of using different IPCC emissions scenarios can be large or small, depending on the specific scenarios.

(5) The projections that best reproduce the recent change suggest that the current trend towards higher winter inflows and lower spring flood will continue in the period 2009–2030.

The significance and validity of these results must, however, be viewed in light of the main limitations of the study.

(1) Only one catchment is studied.

(2) The recent change is estimated using 19 years of data, which is admittedly a rather short period in this context.

(3) Although we have a total ensemble of 12 projections, only two to three members are available for assessing each of the uncertainty sources considered.

In light of the latter limitation in particular, the results from the uncertainty source assessment must be interpreted with caution, but for large catchments the properties of the driving GCM seems to dominate the hydrological response in terms of mean annual cycle. It thus appears important to include different GCMs, and notably different GCM initializations, in an ensemble of projections used for hydrological impact assessment. Concerning IPCC emissions scenarios, the results indicate that the spread among projections depend on the specific scenarios used, that is it is important not only to include different scenarios but also to

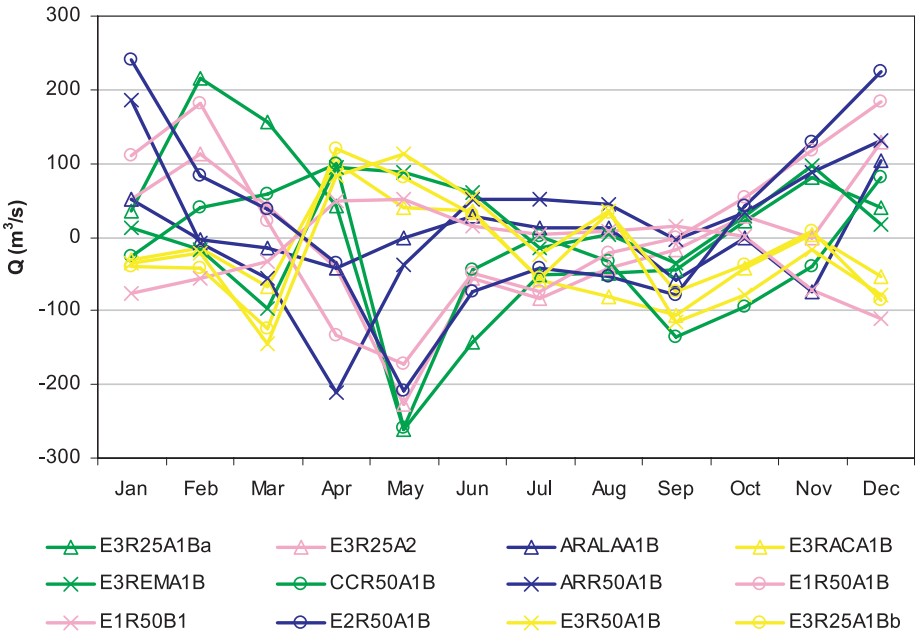

Fig. 9. Projected difference in mean monthly inflow for 2009–2030 compared to 1991–2008. The colours indicate the rank $R_{\Delta 91-08}$ (Table 3) in increasing order: blue (1–3), green (4–6), yellow (7–9), red (10–12). Within each group, a circle denotes lowest rank, triangle intermediate and cross highest rank.

identify the most influential ones. However, natural variability also has an effect, particularly in the early years of the emissions scenarios. The RCM used and its resolution had smaller influence in this study.

The striking differences between ensemble members from the same GCM indicate the crucial impact of GCM initialization on its ability to reproduce historical changes. This is further evidence of the importance that the role of natural variability within the models plays on the climate projections. Whereas GCMs may be shown to climatologically represent global circulation patterns, this does not imply that interannual variability will be in phase with historical periods. This underlines the importance of ongoing development of earth system models that are in phase with the historical climate and thus potentially able to deliver decadal forecasts rather than projections.

It should be noted that additional uncertainty sources, not covered in this study, exist in the modelling of hydrological climate change impacts. One concerns the choice of bias-correction method (Section 3.1.2), which is likely to influence the results. Another source is the hydrological model. Different process descriptions can potentially give quite different responses to projected changes in temperature and precipitation, for example calculation of evapotranspiration. These are important areas of future research. However, as all hydrological simulations in this study were treated in the same, consistent manner, these uncertainties would not likely have a major impact on the conclusions made here.

To conclude, the study shows that climate models are able to reproduce not only the hydrological regime in the commonly used control period 1961–1990 but also key aspects of the changes observed since 1990. The ability to accurately reproduce these changes, however, differs between projections. Evaluation techniques along the lines suggested in this paper provide a potential way to improve accuracy and confidence in near-future projections.

6. Acknowledgments

Many of the climate model projections came from the ENSEMBLES Project, funded by the European Commission's 6th Framework Programme through contract GOCE-CT-2003-505539). Others were provided by the Rossby Centre at SMHI. The work was funded in part by ENSEMBLES, the SAWA and CPA Projects under the EU Interreg IVB North Sea Region Programme, the SWECIA Programme under Mistra (the Foundation for Strategic Environmental Research) and the Swedish Research Council Formas. We thank Vattenfall AB for allowing the operational HBV Model for Lake Vänern to be used in this study.

References

Andréasson, J., Bergström, S., Carlsson, B., Graham, L. P. and Lindström, G. 2004. Hydrological change—climate change impact simulations for Sweden. *Ambio.* **33**, 228–234.

Arheimer, B. and Brandt, M. 1998. Modelling nitrogen transport and retention in the catchments of southern Sweden. *Ambio.* **27**, 471–480.

Arheimer, B., Andréasson, J., Fogelberg, S., Johnsson, H., Pers, B. C. and co-authors. 2005. Climate change impact on water quality: model results from southern Sweden. *Ambio.* **34**, 559–566.

Bergström, S. 1976. *Development and application of a conceptual runoff model for Scandinavian catchments*. SMHI Reports Hydrology and Oceanography, No. 7, 134.

Bergström, S. 1992. *The HBV model–its structure and applications*. SMHI Reports Hydrology, No. 4, 35.

Bergström, S., Harlin, J. and Lindström, G. 1992. Spillway design floods in Sweden. I: New guidelines. *Hydrol. Sci. J.* **37**, 505–519.

Bergström, S., Carlsson, B., Gardelin, M., Lindström, G., Pettersson, A. and co-authors. 2001. Climate change impacts on runoff in Sweden–assessments by global climate models, dynamical downscaling and hydrological modelling. *Climate Res.* **16**, 101–112.

Bergström, S., Hellström, S.-S. and Andréasson, J. 2007. Future flood risks around the big Swedish lakes. In: *Proceedings of the 3rd International Conference on Climate and Water* (ed. M. Heinonen), Finnish Environment Institute, Helsinki, 63–68.

Déqué, M., Rowell, D. P., Lüthi, D., Giorgi, F., Christensen, J. H. and co-authors. 2007. An intercomparison of regional climate simulations for Europe: assessing uncertainties in model projections. *Climatic Change* **81**, 53–70.

Graham, P., 1999. Modelling runoff to the Baltic basin. *Ambio.* **28**, 328–334.

Graham, L.P., Andréasson, J. and Carlsson, B. 2007a. Assessing climate change impacts on hydrology from an ensemble of regional climate models, model scales and linking methods—a case study on the Lule River Basin. *Climatic Change* **81**, 293–307.

Graham, L. P., Hagemann, S., Jaun, S. and Beniston, M. 2007b. On interpreting hydrological change from regional climate models. *Climatic Change* **81**, 97–122.

IPCC. 2007. Summary for Policymakers. In: *Climate Change 2007: The Physical Science Basis. Contribution of Working Group I to the Fourth Assessment Report of the Intergovernmental Panel on Climate Change* (eds S. Solomon, D. Qin, M. Manning, Z. Chen, M. Marquis, K. B. Averyt, M. Tignor, and H. L. Miller), Cambridge University Press, Cambridge, United Kingdom and New York, NY, USA.

Jacob, D., Bärring, L., Christensen, O. B., Christensen, J. H., de Castro, M. and co-authors. 2007. An intercomparison of regional climate models for Europe: model performance in present-day climate. *Climatic Change* **81**, 31–52.

Johansson, B. 2000. Areal precipitation and temperature in the Swedish mountains. An evaluation from a hydrological perspective. *Nord. Hydrol.* **31**, 207–228.

Johansson, B. and Chen, D. 2003. The influence of wind and topography on precipitation distribution in Sweden: statistical analysis and modelling. *Int. J. Climatol.* **23**, 1523–1535.

Kjellström, K., Hansson, U., Jones, C., Nikulin, G., Strandberg G. and co-authors. 2010. 21st century changes in the European climate: uncertainties derived from an ensemble of regional climate model simulations. *Tellus* **63A**, 24–40.

Lilliefors, H. W. 1967. On the Kolmogorov-Smirnov test for normality with mean and variance unknown. *J. Am. Stat. Assoc.* **62**, 399–402.

Lindström, G. and Rodhe, A. 1992. Transit times of water in soil lysimeters from modelling of oxygen-18. *Water Air Soil Poll*. **65**, 83–100.

Lindström, G., Gardelin, M. and Persson, M., 1994. *Conceptual Modelling of Evapotranspiration for Simulations of Climate Change Effects*. SMHI Reports Hydrology, No. 10, Swedish Meteorological and Hydrological Institute, Norrköping, Sweden, 25.

Lindström, G., Johansson, B., Persson, M., Gardelin, M. and Bergström, S. 1997. Development and test of the distributed HBV-96 hydrological model. *J. Hydrol.* **201**, 272–288.

SOU. 2007. *Sweden facing climate change: threats and opportunities*. Final Report from the Swedish Commission on Climate and Vulnerability. Statens Offentliga Utredningar, 2007:60. Fritze, Stockholm.

Van Der Linden, P. and Mitchell, J. F. B. (eds.), 2009. *ENSEMBLES: climate change and its impacts: summary of research and results from the ENSEMBLES project*. Met Office Hadley Centre, Exeter, UK, 160.

Wilks, D. S. 1995. *Statistical Models in the Atmospheric Sciences*. Academic, San Diego.

Yang, W., Andréasson, J., Graham, L. P., Olsson, J., Rosberg, J. and Wetterhall, F. 2010. Improved use of RCM simulations in hydrological climate change impact studies. *Hydrol. Res.* **41**, 211–229.